

# Self-consistent transport simulation of boron dust particle injection in the peripheral plasma in Large Helical Device

メタデータ	言語: en 出版者: Wiley 公開日: 2024-04-03 キーワード (Ja): キーワード (En): 作成者: SHOJI, Mamoru, KAWAMURA, Gakushi, SMIRNOV, Roman, TANAKA, Yasunori, MASUZAKI, Suguru, NESPOLI, Federico, GILSON, Eric, LUNSFORD, Robert メールアドレス: 所属:
URL	<a href="http://hdl.handle.net/10655/0002000460">http://hdl.handle.net/10655/0002000460</a>

This work is licensed under a Creative Commons Attribution-NonCommercial-ShareAlike 4.0 International License.



# Self-consistent transport simulation of boron dust particle injection in the peripheral plasma in Large Helical Device

M. Shoji<sup>1,2</sup> | G. Kawamura<sup>1,2</sup> | R. Smirnov<sup>3</sup> | Y. Tanaka<sup>4</sup> | S. Masuzaki<sup>1,2</sup> |  
F. Nespoli<sup>5</sup> | E. Gilson<sup>5</sup> | R. Lunsford<sup>5</sup>

<sup>1</sup>National Institute for Fusion Science, National Institutes of Natural Sciences, Gifu, Japan

<sup>2</sup>Fusion Science Program, Graduate University for Advanced Studies (SOKENDAI), Hayama, Japan

<sup>3</sup>Department of Mechanical and Aerospace Engineering, University of California at San Diego, La Jolla, California, USA

<sup>4</sup>Institute of Science and Engineering, Kanazawa University, Kanazawa, Japan

<sup>5</sup>Department of Energy National Laboratory, Princeton Plasma Physics Laboratory, Princeton, New Jersey, USA

## Correspondence

M. Shoji, National Institute for Fusion Science, National Institutes of Natural Sciences, Oroshi-cho, Toki, Gifu 509-5292, Japan.

Email: [shohji.mamoru@nifs.ac.jp](mailto:shohji.mamoru@nifs.ac.jp)

## Funding information

NIFS Collaboration Research Program, Grant/Award Number: NIFS20KIST004; Japan Society for the Promotion of Science KAKENHI, Grant/Award Number: 21K18620; U.S. Department of Energy, Grant/Award Number: DE-AC02-09CH11466

## Abstract

The trajectories and the ablation positions of boron dust particles dropped from an impurity powder dropper in the peripheral plasma in the Large Helical Device (LHD) were calculated using a three-dimensional edge plasma simulation code (EMC3-EIRENE) and a dust transport simulation code (DUSTT). The simulation shows that the trajectory of the boron dust particles is deflected at the upper divertor leg due to the effect of the hydrogen plasma flow, and the ablation positions of the dust particles in an ergodic layer change toward the outboard side of the torus for higher plasma densities. The effect of the boron ion flow in the divertor leg on the deflection is investigated by coupling the two codes self-consistently. The simulation predicts that the boron ions in the divertor leg, which are produced by sputtering on the divertor plates, which do not affect the change in the ablation positions. It also shows that the ablation positions move toward the inboard side and approach the Last Closed Flux Surface (LCFS) in case of increased boron dust drop rates, which is caused by the lowered plasma flow in the upper divertor leg due to the lowered electron temperature by radiation cooling by the dropped dust particles.

## KEYWORDS

dust particle transport, DUSTT, EMC3-EIRENE, impurity powder dropper, LHD

## 1 | INTRODUCTION

Impurity powder injection is an attractive optional technique for impurity seeding, wall conditioning, and dust transport studies in magnetic plasma confinement devices.<sup>[1]</sup> A multi-species impurity powder dropper (IPD)<sup>[2]</sup> was installed at an upper port on the vacuum vessel in the Large Helical Device (LHD).<sup>[3]</sup> Boron dust particles were dropped by the IPD in previous experimental campaigns, which demonstrated the improvement of ion and electron energy confinement in LHD plasmas.<sup>[4,5]</sup> The experimental results indicated that the control of the trajectory and the ablation positions of the dropped dust particles in the peripheral plasma are critical issues for realizing high-performance plasma discharges.<sup>[6]</sup> Simulation analyses using a three-dimensional edge plasma simulation code (EMC3-EIRENE)<sup>[7,8]</sup> and a dust transport

This is an open access article under the terms of the [Creative Commons Attribution](https://creativecommons.org/licenses/by/4.0/) License, which permits use, distribution and reproduction in any medium, provided the original work is properly cited.

© 2024 The Authors. *Contributions to Plasma Physics* published by Wiley-VCH GmbH.

simulation code (DUSTT)<sup>[9–11]</sup> proved that the effect of the plasma flow in an upper divertor leg deflects the trajectories of the dropped dust particles,<sup>[12]</sup> which can disturb the control of the ablation positions of the dust particles and the impurity source profile in the peripheral plasma. The previous simulation was performed by assuming that the background plasma parameter profiles were fixed and the density of the impurity ions originating from the dust particles was negligible compared with that of the plasma. This assumption is only valid for the cases of quite low impurity densities in the peripheral plasma and much lower dust drop rates. In order to extend the applicability of the simulation analysis, a self-consistent simulation by coupling EMC3-EIRENE with DUSTT was developed, which provides calculations that are consistent in both codes under conditions where the impurity ion densities are not negligible. In the following section, the setup for the self-consistent simulation and calculations are presented. The effect of the impurity ions in the peripheral plasma on the dropped dust particle trajectories is investigated from two points of view. One is the effect of boron atoms produced by sputtering on the divertor plates due to the plasma (hydrogen ions), and the other is that by the boron ions originating from the dropped boron dust particles.

## 2 | SETUP FOR SELF-CONSISTENT SIMULATION OF THREE-DIMENSIONAL DUST PARTICLE TRAJECTORIES

Figure 1 shows a perspective of a three-dimensional model for simulating the trajectories of dust particles dropped by the IPD, which is for a half helical section ( $18^\circ$  in toroidal direction) of the vacuum vessel in an open divertor configuration in the LHD. The plasma parameter profiles in the peripheral plasma (including the ergodic layer and four divertor legs) are provided by a three-dimensional edge plasma simulation code (EMC3-EIRENE). It surrounds the main plasma confinement region inside the Last Closed Flux Surface (LCFS) for a typical magnetic configuration (the radial position of the magnetic axis  $R_{ax} = 3.60$  m). The EMC3-EIRENE code also calculates the density profile of the impurity ions in the peripheral plasma by solving the continuity and the momentum balance equations of the impurity ions for each ionization stage under the assumption that the temperature of the impurity ions equals the ion temperature of the plasma. The ionization/recombination coefficients and the radiation power of the impurity ions are derived from the Atomic Data and Analysis Structure (ADAS).<sup>[13]</sup> The plasma heating power and the plasma density at the LCFS ( $P^{LCFS}$  and  $n_e^{LCFS}$ ) are primary input parameters for EMC3-EIRENE. The energy and particle diffusion coefficients in the plasma were set to 0.5 and 1.0  $m^2/s$ , respectively, and the particle diffusion coefficient of the impurity ions was fixed to 1.0  $m^2/s$ . These coefficients are typical values for reproducing the observed radial profile of the electron temperature, electron density, and impurity ion density in the peripheral plasmas. A helical symmetry of the spatial profile of the plasma and impurities is assumed at both toroidal ends of the three-dimensional model.

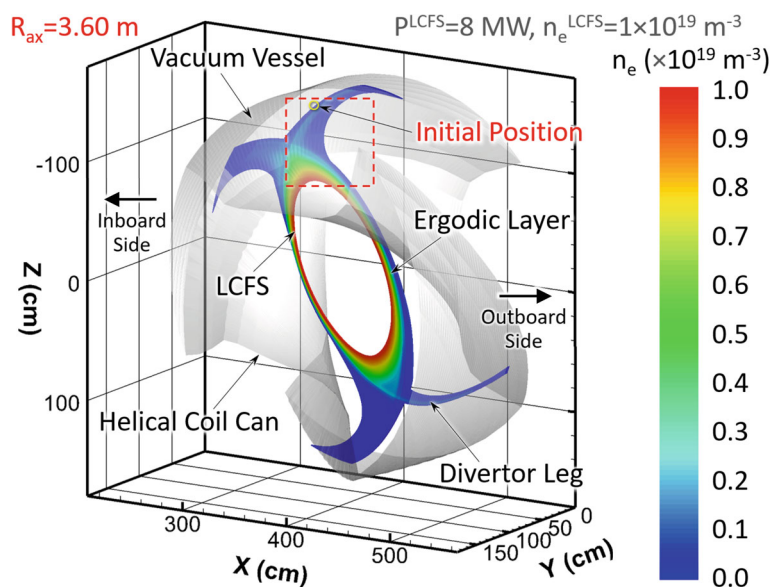


**FIGURE 1** A perspective of a three-dimensional model for the dust transport simulation for a half helical section in the open divertor configuration in the case of  $R_{ax} = 3.60$  m,  $P^{LCFS} = 8$  MW, and  $n_e^{LCFS} = 4 \times 10^{19} m^{-3}$ .

The initial position of the boron dust particles dropped from the IPD was set just above the upper divertor leg, as indicated by an open yellow circle in Figure 1. The dust particles are injected downward from this position in free fall at an initial velocity of 5 m/s, which corresponds to the actual velocity when the dust particles are dropped from the IPD installation position at the upper port (outside of the model). The trajectories of the dust particles are calculated using a dust transport simulation code (DUSTT) in the background plasma provided by EMC3-EIRENE. The DUSTT code calculates the dust particle trajectories by solving the equation of motion, mass, energy, and electric potential of the dust particles. In this simulation, the force acting on a dust particle is the sum of the friction force by ions and neutrals, electric force, and gravity force. Others such as the Lorentz force, electron drag, thermophoretic, rocket, and radiation pressure forces are not included because of their mild influences on the dust particle trajectories. The friction force between dust and ion particles has two components. One is the force caused by the absorption of ions by dust particles, which is calculated by employing the orbital motion limited (OML) theory.<sup>[14]</sup> The other one is due to Coulomb's scattering between ions and dust particles. The DUSTT code assumes that the dust particles are composed of a single atomic element (boron) and the shape is spherical. This code provides a three-dimensional profile of the production rate of the neutral impurity atoms originating from the dust particles evaporated or sublimated by the plasma heat load. For simplicity, the reflection of the dust particles on the surface of the vacuum vessel (stainless steel) and the divertor plates (carbon) is not included in the simulation. A converged solution of the plasma parameter profile and the dust particle trajectory is finally obtained using an iterative calculation scheme between EMC3-EIRENE and DUSTT. It should be noted that the EMC3-EIRENE code assumes a much lower impurity ion density content in the plasma, although the radiation power by impurity ions is included in the energy balance equation. The appropriateness of the assumption of the low impurity ion content will be verified in the following sections.

In the previous paper, the dust particle trajectories were calculated assuming that the background plasma parameters were fixed, and the effect of the impurity ions in the peripheral plasma was negligible.<sup>[12]</sup> These assumptions are not appropriate in cases of high sputtering rates of impurities on the divertor plates and higher dust particle dropping rates. In these cases, the effect of the impurity ion flow in the peripheral plasma can influence the dust particle trajectories, which leads to a change in the ablation positions of the dust particles and the impurity source profile. Thus, the impurity ions have to be considered to extend the applicability of the simulation analysis. There are two major possible processes for impurity sources in plasma discharge experiments with the boron dust particle injection. One is the boron atoms produced by sputtering on the divertor plates due to incident hydrogen ions in the plasma. A multichannel spectrometer detected a boron source in the front of the divertor plates in the inboard side of the torus.<sup>[15]</sup> The boron ion flow produced by the ionization of the sputtered boron atoms in the divertor legs can affect the dust trajectories. The other one is the boron ion flow induced by the ionization of the boron atoms evaporated from the dropped boron dust particles. The flow of the boron ions transported to the divertor legs can contribute to the deflection of the dust trajectories. In this simulation, the sputtering of carbon atoms on the divertor plates by the plasma is ignored to focus on the effect of the boron ion flow on the deflection of the boron dust trajectories. In the following sections, the effect of the two impurity sources on the dust particle trajectories is investigated using EMC3-EIRENE and DUSTT.

### 3 | EFFECT OF SPUTTERING OF BORON ON DROPPED DUST PARTICLE TRAJECTORIES

The effect of the sputtering of boron on the divertor plates was investigated using a new iterative calculation scheme between the two codes. The multichannel spectroscopic measurement in the plasma discharges with boron dust particle injection demonstrated the localized emission of singly charged boron ions and boron hydride molecules in the closed helical divertor region in the inboard side of the torus.<sup>[15]</sup> The measurement indicates that boron atoms are deposited and accumulated on the divertor plates, and they are sputtered by the plasma (hydrogen ions) on the divertor plates. The sputtered boron atoms are ionized in the peripheral plasma to produce the boron ion flow in the divertor legs. The effect of the boron ion flow should be numerically investigated using the simulation codes to predict the ablation positions of the boron dust particles in higher boron density conditions in the peripheral plasma. This effect was investigated by changing the sputtering rate of boron on the divertor plates, which is one of the control parameters in the EMC3-EIRENE code. In this simulation, the effect of reflected boron atoms and the self-sputtering of boron on the divertor plates are not included for simple calculation. These are reasonable approximations because of the low flux density of boron ions on the divertor plates compared with that of hydrogen ions. Figure 2 shows the dependence of the boron dust particle trajectories on the sputtering rates of boron ( $R_{sp}^B$ ), in which the diameter of the boron dust particle was set to 150  $\mu\text{m}$ , which is the

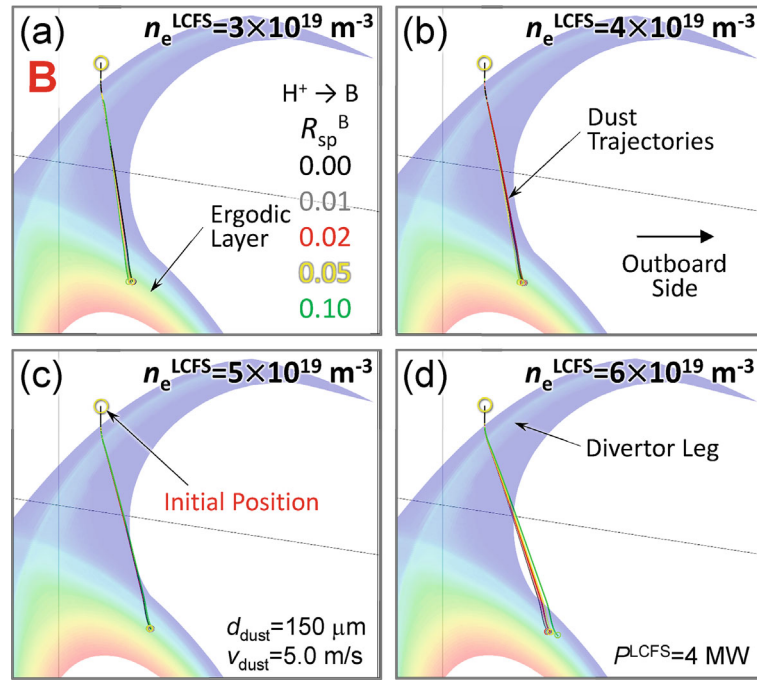


**FIGURE 2** The dependence of the boron dust particle trajectories on the boron sputtering rates on the divertor plates for (a)  $n_e^{\text{LCFS}} = 3 \times 10^{19} \text{ m}^{-3}$ , (b)  $n_e^{\text{LCFS}} = 4 \times 10^{19} \text{ m}^{-3}$ , (c)  $n_e^{\text{LCFS}} = 5 \times 10^{19} \text{ m}^{-3}$ , and (d)  $n_e^{\text{LCFS}} = 6 \times 10^{19} \text{ m}^{-3}$ . The diameter of the dropped boron dust particle is set to  $150 \mu\text{m}$ , the parameter  $P^{\text{LCFS}}$  is set to  $4 \text{ MW}$ , and the sputtering rate is changed from 0 to 0.10. The ablation positions of the dropped boron dust particles are indicated as colored open circles.

nominal diameter of the boron dust particles used in the LHD. In these simulations, the dust drop rate was set to a quite small value, which is too small to contribute to the boron ion density in the peripheral plasma. The parameter  $P^{\text{LCFS}}$  was set to  $4 \text{ MW}$ , and  $n_e^{\text{LCFS}}$  values were varied from  $3 \times 10^{19}$  to  $6 \times 10^{19} \text{ m}^{-3}$ , which are typical ones in the plasma discharge experiments using the IPD. The most probable incident energy of hydrogen ions onto the divertor plates is about  $100 \text{ eV}$  because the typical electron temperature at the strike points on the divertor plates is about  $30 \text{ eV}$  in the LHD.<sup>[16]</sup> The boron sputtering rate was artificially changed from 0 to 0.10, where the typical sputtering rate of boron by incident hydrogen ions is estimated to be about 0.01 in the case where pure boron layers are formed on the divertor plates.<sup>[17]</sup> The figure shows that the trajectories of the dropped boron dust particles are more deflected for higher plasma densities by the effect of the plasma flow in the upper divertor leg, which has already been reported in the previous simulations.<sup>[12]</sup> It proves that the change in the sputtering rate does not significantly affect the boron dust trajectories. In this simulation, the ablation position is defined as the points where the dropped boron dust particles are completely evaporated. This figure shows no observable change in the ablation positions in the ergodic layer as indicated by colored open circles.

The simulations showed that singly charged boron ions are dominant in the divertor region. Figure 3a presents the density profile of the boron ions in the upper divertor leg, which shows the locally high boron ion density at the downstream side of the upper divertor leg close to the divertor plates (the upper-right corner in this figure), which is caused by the ionization of the sputtered boron atoms. Figure 3b,c presents the profile of the plasma density and the plasma flow velocity for a boron sputtering rate of 0.10 and  $n_e^{\text{LCFS}} = 6 \times 10^{19} \text{ m}^{-3}$ , respectively. The upstream and downstream flow velocities along the magnetic field lines in the divertor leg are indicated in red and blue, respectively. The singly charged boron ion density in the upper divertor leg is about 2% of the plasma density, even in the highest boron sputtering rate case, demonstrating the appropriateness of the assumption adopted in the EMC3-EIRENE code. It was found that the boron ion density in the divertor leg rapidly decreases with the charge numbers, and the flow velocities of the boron ions are almost equivalent to the plasma flow velocity. The boron ion density is much smaller than the plasma density with the equivalent flow velocities, meaning that the frictional force on the dust particles by the boron ion flow in the upper divertor leg is negligible compared with that by the plasma flow. The simulation demonstrates that the boron atoms sputtered from the divertor plates have no observable influence on the change in the dropped boron dust particle trajectories, even in the highest sputtering rate of 0.10.

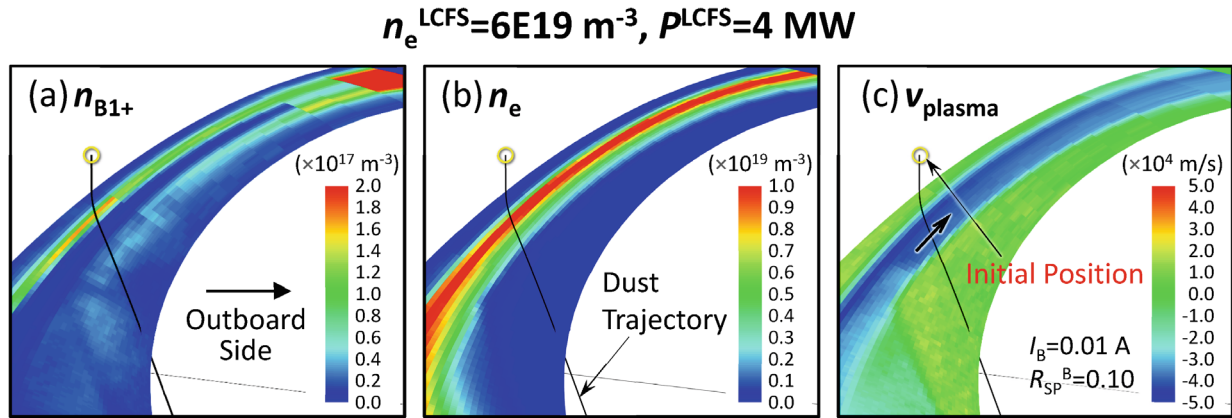


**FIGURE 3** (a) The density profile of the singly charged boron ions in the upper divertor leg, which shows the locally high boron ion density near the divertor plates (the upper-right corner in this figure), (b) the profile of the plasma density, and (c) the profile of the plasma flow velocity for the highest boron sputtering rate of 0.10 in the case of  $R_{\text{ax}} = 3.60 \text{ m}$ ,  $P^{\text{LCFS}} = 4 \text{ MW}$ , and  $n_e^{\text{LCFS}} = 6 \times 10^{19} \text{ m}^{-3}$ . The negative values in Figure (c) indicate the flow velocities with the direction to the divertor plates along the magnetic field lines (downstream). The diameter of the boron dust particle is set to  $150 \mu\text{m}$ .

#### 4 | EFFECT OF BORON ION FLOW INDUCED BY DROPPED DUST PARTICLES ON DUST TRAJECTORIES

The trajectories of the dropped boron dust particles can be affected by the boron ion flow in the upper divertor leg, which is produced by the dropped boron dust particles itself in the ergodic layer. There is a possibility that the boron ion flow contributes to the deflection of the dust trajectory toward the outboard side because of the outward boron ion flow in the upper divertor leg. Thus, a newer version of the DUSTT code, which is able to include the effect of the impurity ions in the plasma, was applied to investigate this possibility.<sup>[18]</sup> Figure 4 depicts the dependence of the ablation positions of the boron dust particles on the dust drop rate for the four plasma densities ( $n_e^{\text{LCFS}} = 3 \times 10^{19}$ ,  $4 \times 10^{19}$ ,  $5 \times 10^{19}$ , and  $6 \times 10^{19} \text{ m}^{-3}$ ), with  $P^{\text{LCFS}} = 4 \text{ MW}$ . Here, the dust drop rate ( $I_B$ ) is defined as the number of boron atoms injected into the plasma per second as the dust particles. The sputtering of boron atoms on the divertor plates is not included for simplicity. The simulation demonstrates the suppression of the deflection of the boron dust trajectories with the increase in the dust drop rate, and the ablation positions move toward the inboard side and approach the LCFS in the ergodic layer for the higher dust drop rates.

The simulation showed that the density of the boron ions in the upper divertor leg is much lower than the plasma density even in a high dust drop rate of  $2.5 \times 10^{20}$  (atoms/s) by about two orders of magnitude, which results in no significant contribution to the deflection of the dust trajectory because of the comparable flow velocity of the boron ions to that of the plasma in the divertor leg. Figure 5 displays the dependence of the plasma flow velocity and the electron temperature in the upper divertor leg on the dust drop rate. As shown in this figure, the absolute plasma flow velocity decreases with the dust drop rate, which is caused by the lowered electron/ion temperature in the peripheral plasma, due to the radiation cooling in the ergodic layer by the dropped boron dust particles. The simulations of the total radiation power of the boron ions in the peripheral plasma for the three dust drop rates ( $I_B = 6.2 \times 10^{16}$ ,  $1.3 \times 10^{20}$ , and  $2.5 \times 10^{20}$  atoms/s) are  $2.4 \times 10^1$ ,  $6.5 \times 10^4$ , and  $8.8 \times 10^4 \text{ W}$  for a half helical section, respectively. The move of the ablation positions toward the inboard side of the torus with the increase in the dust drop rate is explained by the suppression of the deflection of the dust trajectory. It is mainly caused by the decrease in the absolute plasma flow velocity in the upper divertor leg. As for the movement of the ablation positions to the LCFS in higher dust drop rates, it is explained by the lowered plasma temperature in the ergodic layer by radiation cooling due to the dropped boron dust particles. The effect of the change in the collisionality between the dust particles and the plasma is considered in the self-consistent simulation, which changes the dust particle trajectory just as a secondary effect. The simulations will provide a useful guideline to control the position of the boron ion source and to optimize the boron dust drop rate for effectively applying the IPD to plasma discharge experiments in the LHD.

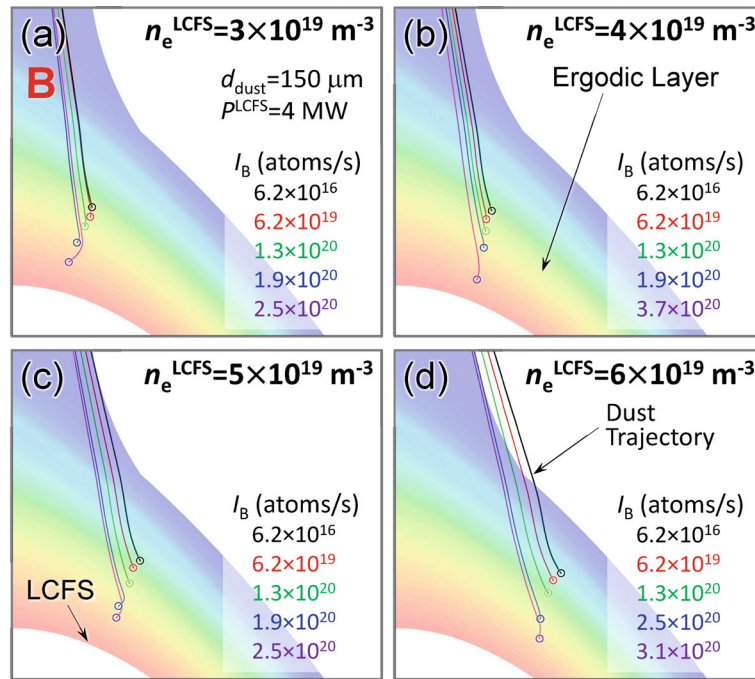


**FIGURE 4** Enlarged images showing the dependence of the ablation positions of the boron dust particles on the dust drop rate for (a)  $n_e^{\text{LCFS}} = 3 \times 10^{19} \text{ m}^{-3}$ , (b)  $n_e^{\text{LCFS}} = 4 \times 10^{19} \text{ m}^{-3}$ , (c)  $n_e^{\text{LCFS}} = 5 \times 10^{19} \text{ m}^{-3}$ , and (d)  $n_e^{\text{LCFS}} = 6 \times 10^{19} \text{ m}^{-3}$  with  $p^{\text{LCFS}} = 4 \text{ MW}$ . The diameter of the boron dust particle is set to  $150 \mu\text{m}$ . The ablation positions of the dropped boron dust particles are indicated as colored open circles.

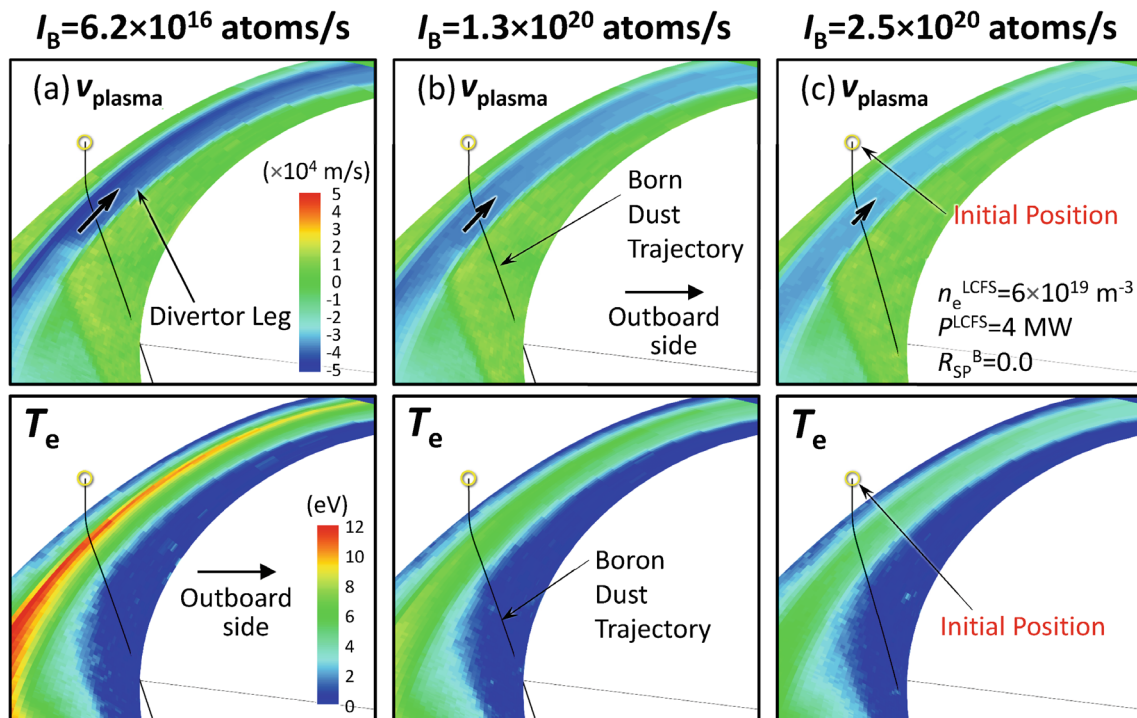


**FIGURE 5** Variation in the profile of the plasma flow velocity and the electron temperature in the upper divertor leg for three boron dust drop rates for (a)  $6.2 \times 10^{16}$ , (b)  $1.3 \times 10^{20}$ , and (c)  $2.5 \times 10^{20}$  atoms/s in the case of  $R_{\text{ax}} = 3.60 \text{ m}$ ,  $p^{\text{LCFS}} = 4 \text{ MW}$ , and  $n_e^{\text{LCFS}} = 6 \times 10^{19} \text{ m}^{-3}$ .

## 5 | SUMMARY

The self-consistent simulation coupling of EMC3-EIRENE with DUSTT was developed to investigate the effect of the boron ion flow in the peripheral plasma on the boron dust trajectory dropped from the IPD. It revealed that the sputtering of boron atoms on the divertor plates does not significantly change the boron dust particle trajectories. This is because of the much lower density of boron ions than the plasma density in the upper divertor leg, even in the highest sputtering rate. The simulation predicts that the deflection of the dropped boron dust trajectory is suppressed with the increase in the dust drop rate, in which the effect of the boron ion flow is much lower than that of the plasma flow, even in the case of the highest dust drop rate. The simulation reveals that the ablation positions move toward the inboard side and approach the LCFS in the ergodic layer with the increase in the dust drop rate, which is caused by the decrease in the absolute plasma flow velocity in the upper divertor leg, due to the lowered electron/ion temperature, by the radiation cooling induced by the dropped boron dust particles in the ergodic layer.

## ACKNOWLEDGMENTS

This work was performed under the auspices of the NIFS Collaboration Research Program (NIFS20KIST004). One of the authors (M. S.) would like to thank Y. Feng for permission to use EMC3-EIRENE. He is also grateful for the computational resources of the plasma simulator in NIFS. This work is supported by Japan Society for the Promotion of Science KAKENHI Grant Number 21K18620. This work is also supported by the U.S. Department of Energy under Contract. No. DE-AC02-09CH11466 with Princeton University”.

## DATA AVAILABILITY STATEMENT

The data that support the findings of this study are openly available in LHD experiment data repository at [https://www.lhd.nifs.ac.jp/pub/Repository\\_en.html](https://www.lhd.nifs.ac.jp/pub/Repository_en.html).

## REFERENCES

- [1] A. Bortolon, V. Rohde, R. Maingi, E. Wolfrum, R. Dux, A. Herrmann, R. Lunsford, R. M. McDermott, A. Nagy, A. Kallenbach, D. K. Mansfield, R. Nazikian, R. Neu, *Nucl. Mater. Energy* **2019**, *19*, 384.
- [2] A. Nagy, A. Bortolon, D. M. Mauzey, E. Wolfe, E. P. Gilson, R. Lunsford, R. Maingi, D. K. Mansfield, R. Nazikian, A. L. Roquemore, *Rev. Sci. Instrum.* **2018**, *89*, 10K121.
- [3] Y. Takeiri, T. Morisaki, M. Osakabe, M. Yokoyama, S. Sakakibara, H. Takahashi, Y. Nakamura, T. Oishi, G. Motojima, S. Murakami, K. Ito, A. Ejiri, S. Imagawa, S. Inagaki, M. Isobe, S. K. S. Masamune, T. Mito, I. Murakami, K. Nagaoka, K. Nagasaki, K. Nishimura, M. Sakamoto, R. Sakamoto, T. Shimozuma, K. Shinohara, H. Sugama, K. Y. Watanabe, J. W. Ahn, N. Akata, T. Akiyama, N. Ashikawa, J. Baldzuhn, T. Bando, E. Bernard, F. Castejón, H. Chikaraishi, M. Emoto, T. Evans, N. Ezumi, K. Fujii, H. Funaba, M. Goto, T. Goto, D. Gradic, Y. Gunsu, S. Hamaguchi, H. Hasegawa, Y. Hayashi, C. Hidalgo, T. Higashiguchi, Y. Hirooka, Y. Hishinuma, R. Horiuchi, K. Ichiguchi, K. Ida, T. Ido, H. Igami, K. Ikeda, S. Ishiguro, R. Ishizaki, A. Ishizawa, A. Ito, Y. Ito, A. Iwamoto, S. Kamio, K. Kamiya, O. Kaneko, R. Kanno, H. Kashara, D. Kato, T. Kato, K. Kawahata, G. Kawamura, M. Kasaki, S. Kitajima, W. H. Ko, M. Kobayashi, S. Kobayashi, T. Kobayashi, K. Koga, A. Kohyama, R. Kumazawa, J. H. Lee, D. López-Bruna, R. Makino, S. Masuzaki, Y. Matsumoto, H. Matsuura, O. Mitarai, H. Miura, J. Miyazawa, N. Mizuguchi, C. Moon, S. Morita, T. Moritaka, K. Mukai, T. Muroga, S. Muto, T. Mutoh, T. Nagasaka, Y. Nagayama, N. Nakajima, Y. Nakamura, H. Nakanishi, H. Nakano, M. Nakata, Y. Narushima, D. Nishijima, A. Nishimura, S. Nishimura, T. Nishitani, M. Nishiura, Y. Nobuta, H. Noto, M. Nunami, T. Obana, K. Ogawa, S. Ohdachi, M. Ohno, N. Ohno, H. Ohtani, M. Okamoto, Y. Oya, T. Ozaki, B. J. Peterson, M. Preynas, S. Sagara, K. Saito, H. Sakaue, A. Sanpei, S. Satake, M. Sato, T. Saze, O. Schmitz, R. Seki, T. Seki, I. Sharov, A. Shimizu, M. Shiratani, M. Shoji, C. Skinner, R. Soga, T. Stange, C. Suzuki, Y. Suzuki, S. Takada, K. Takahata, A. Takayama, S. Takayama, Y. Takemura, Y. Takeuchi, H. Tamura, N. Tamura, H. Tanaka, K. Tanaka, M. Tanaka, T. Tanaka, Y. Tanaka, S. Toda, Y. Todo, K. Toi, M. Toida, M. Tokitani, T. Tokuzawa, H. Tsuchiya, T. Tsujimura, K. Tsumori, S. Usami, J. L. Velasco, H. Wang, T. H. Watanabe, T. Watanabe, J. Yagi, M. Yajima, H. Yamada, I. Yamada, O. Yamagishi, N. Yamaguchi, Y. Yamamoto, N. Yanagi, R. Yasuhara, E. Yatsuka, N. Yoshida, M. Yoshinuma, S. Yoshimura, Y. Yoshimura, *Nucl. Fusion* **2017**, *57*, 102023.
- [4] F. Nespoli, S. Masuzaki, K. Tanaka, N. Ashikawa, M. Shoji, E. P. Gilson, R. Lunsford, T. Oishi, K. Ida, M. Yoshinuma, Y. Takemura, T. Kinoshita, G. Motojima, N. Kenmochi, G. Kawamura, C. Suzuki, A. Nagy, A. Bortolon, N. A. Pablant, A. Mollen, N. Tamura, D. A. Gates, T. Morisaki, *Nat. Phys.* **2022**, *18*, 350.
- [5] F. Nespoli, K. Tanaka, S. Masuzaki, N. Ashikawa, M. Shoji, E. P. Gilson, R. Lunsford, T. Oishi, K. Ida, M. Yoshinuma, Y. Takemura, T. Kinoshita, G. Motojima, M. Osakabe, N. Kenmochi, G. Kawamura, C. Suzuki, A. Nagy, A. Bortolon, N. A. Pablant, A. Mollen, N. Tamura, D. A. Gates, T. Morisaki, *Nucl. Fusion* **2023**, *63*, 076001.
- [6] R. Lunsford, S. Masuzaki, F. Nespoli, N. Ashikawa, E. P. Gilson, D. A. Gates, K. Ida, G. Kawamura, T. Morisaki, A. Nagy, T. Oishi, M. Shoji, C. Suzuki, M. Yoshinuma, *Nucl. Fusion* **2022**, *62*, 086021.
- [7] Y. Feng, F. Sardei, P. Grigull, K. McCormick, J. Kisslinger, D. Reiter, Y. Igitkhanov, *Plasma Phys. Control. Fusion* **2002**, *44*, 611.
- [8] G. Kawamura, Y. Feng, M. Kobayashi, M. Shoji, T. Morisaki, S. Masuzaki, Y. Tomita, *Contrib. Plasma Physics* **2014**, *54*, 437.

- [9] A. Pigarov, S. Krasheninnikov, T. Soboleva, T. Rognlien, *Phys. Plasmas* **2005**, *12*, 122508.
- [10] A. Pigarov, R. Smirnov, S. Krasheninnikov, T. Rognlien, M. Rosenberg, T. Soboleva, *J. Nucl. Mater.* **2007**, 363–365, 216.
- [11] Y. Tanaka, R. Smirnov, A. Pigarov, H. Takenaga, N. Asakura, Y. Uesugi, N. Ohno, *J. Nucl. Mater.* **2011**, *415*, S1106.
- [12] M. Shoji, G. Kawamura, R. Smirnov, Y. Tanaka, S. Masuzaki, Y. Uesugi, N. Ashikawa, E. Gilson, R. Lunsford, *Contrib. Plasma Physics* **2020**, *60*, e201900101.
- [13] The ADAS Project, ADAS Manual 2.6. <https://www.adas.ac.uk/manual.php> August, 2021.
- [14] H. M. Mott-Smith, I. Langmuir, *Phys. Rev.* **1926**, *28*, 727.
- [15] T. Kawate, N. Ashikawa, M. Goto, T. Oishi, Y. Kawamoto, H. Toyoda, M. Shoji, G. Kawamura, S. Masuzaki, F. Nespoli, E. Gilson, R. Lunsford, C. Suzuki, A. Nagy, D. Gates, *Nucl. Fusion* **2022**, *62*, 126052.
- [16] S. Masuzaki, T. Morisaki, N. Ohyabu, A. Komori, H. Suzuki, N. Noda, Y. Kubota, R. Sakamoto, K. Narihara, K. Kawahata, K. Tanaka, T. Tokuzawa, S. Morita, M. Goto, M. Osakabe, T. Watanabe, Y. Matsumoto, O. Motojima, the LHD Experimental group, *Nucl. Fusion* **2002**, *42*, 750.
- [17] W. Möller, W. Eckstein, J. P. Biersack, *Comput. Phys. Commun.* **1988**, *51*, 355.
- [18] R. Smirnov, A. Pigarov, M. Rosenberg, S. Krasheninnikov, D. Mendis, *Plasma Phys. Control Fusion* **2007**, *49*, 347.

**How to cite this article:** M. Shoji, G. Kawamura, R. Smirnov, Y. Tanaka, S. Masuzaki, F. Nespoli, E. Gilson, R. Lunsford, *Contrib. Plasma Phys.* **2024**, e202300105. <https://doi.org/10.1002/ctpp.202300105>